

## Supporting Information

### **Lanthanide-doped LaOBr nanocrystals: controlled synthesis, optical spectroscopy and bioimaging**

Huiqi Wang,<sup>ab</sup> Datao Tu,<sup>\*a</sup> Jin Xu,<sup>a</sup> Xiaoying Shang,<sup>a</sup> Ping Hu,<sup>a</sup> Renfu Li,<sup>a</sup> Wei Zheng,<sup>a</sup> Zhuo Chen,<sup>ab</sup> and Xueyuan Chen<sup>\*ab</sup>

<sup>a</sup> *CAS Key Laboratory of Design and Assembly of Functional Nanostructures, State Key Laboratory of Structural Chemistry, and Fujian Provincial Key Laboratory of Nanomaterials, Fujian Institute of Research on the Structure of Matter, Chinese Academy of Sciences, Fuzhou, Fujian 350002, China.*

<sup>b</sup> *University of Chinese Academy of Sciences, Beijing 100049, China.*

*\* Corresponding author, E-mail: [xchen@fjirsm.ac.cn](mailto:xchen@fjirsm.ac.cn), [dttu@fjirsm.ac.cn](mailto:dttu@fjirsm.ac.cn)*

**Table 1** Theoretically allowed transition lines of  ${}^5D_0 \rightarrow {}^7F_J$  of  $\text{Eu}^{3+}$  ions at 32 crystallographic point groups.

Local symmetry	Point group	The transition lines of ${}^5D_0 \rightarrow {}^7F_J$ ( $J = 0,1,2,3,4,5,6$ )						
		0	1	2	3	4	5	6
Triclinic	$C_1$	1	3	5	7	9	11	13
	$C_i$	0	3	0	0	0	0	0
Monoclinic	$C_s$	1	3	5	7	9	11	13
	$C_2$	1	3	5	7	9	11	13
	$C_{2h}$	0	3	0	0	0	0	0
Orthorhombic	$C_{2v}$	1	3	4	5	7	8	10
	$D_2$	0	3	3	6	6	9	9
	$D_{2h}$	0	3	0	0	0	0	0
Tetragonal	$C_4$	1	2	2	3	5	6	6
	$C_{4v}$	1	2	2	2	4	4	5
	$S_4$	0	2	3	4	4	5	7
	$D_{2d}$	0	2	2	3	3	4	5
	$D_4$	0	2	1	3	3	5	4
	$C_{4h}$	0	2	0	0	0	0	0
	$D_{4h}$	0	2	0	0	0	0	0
Trigonal	$C_3$	1	2	3	5	6	7	9
	$C_{3v}$	1	2	3	3	5	5	7
	$D_3$	0	2	2	4	4	6	6
	$D_{3d}$	0	2	0	0	0	0	0
	$S_6$	0	2	0	0	0	0	0
Hexagonal	$C_6$	1	2	2	2	2	3	5
	$C_{6v}$	1	2	2	1	2	2	4
	$D_6$	0	2	1	2	1	3	3
	$C_{3h}$	0	2	1	3	4	4	4
	$D_{3h}$	0	2	1	2	3	3	3
	$C_{6h}$	0	2	0	0	0	0	0
	$D_{6h}$	0	2	0	0	0	0	0
Cubic	$T$	0	1	1	2	2	3	3
	$T_d$	0	1	1	1	1	1	2
	$T_h$	0	1	0	0	0	0	0
	$O$	0	1	0	1	1	2	1
	$O_h$	0	1	0	0	0	0	0

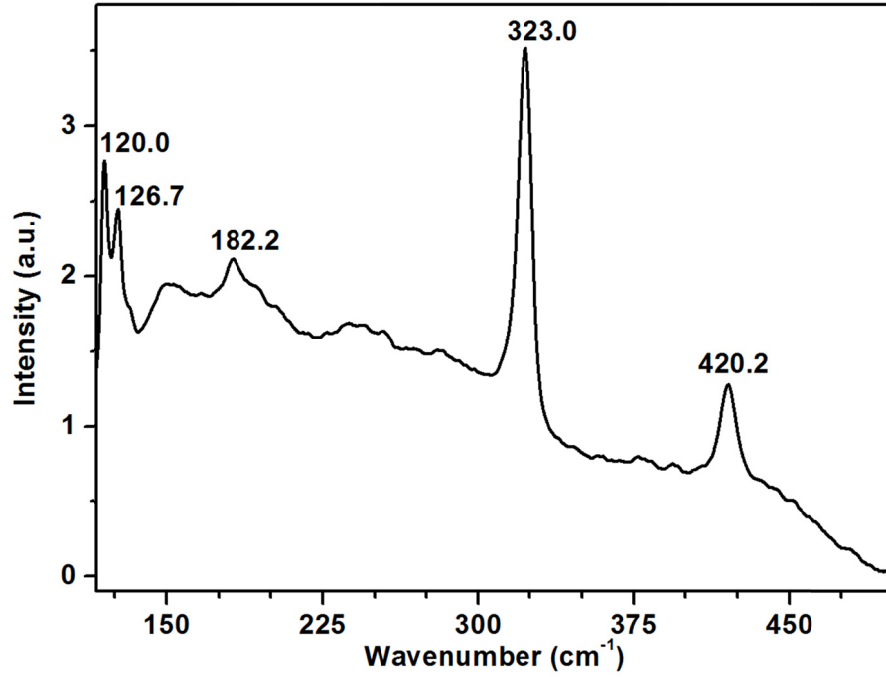


**Fig. S1** Raman spectrum of LaOBr nanocrystals (NCs) upon 785-nm excitation provided by a continuous-wave semiconductor laser diode. It shows five strong peaks at 120.0, 126.7, 182.2, 323.0 and 420.2  $\text{cm}^{-1}$ , which agree well with the lattice vibration energy of tetragonal LaOBr. The maximum phonon energy of 420.2  $\text{cm}^{-1}$  is lower than that of most oxides. As a consequence, photoluminescence (PL) quenching of lanthanide ( $\text{Ln}^{3+}$ ) dopants mediated by nonradiative multiphonon relaxation is relatively weak, indicating that  $\text{Ln}^{3+}$ -doped LaOBr may exhibit high downshifting (DS)/upconversion (UC) luminescence efficiencies.

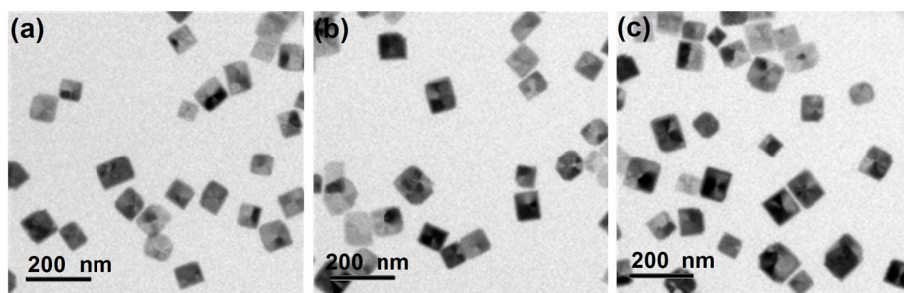


**Fig. S2** TEM images of LaOBr:Yb<sup>3+</sup>/Ho<sup>3+</sup> (x/2 mol%), x = (a) 10, (b) 15, and (c) 20. LaOBr:Yb<sup>3+</sup>/Ho<sup>3+</sup> NCs with different Yb<sup>3+</sup> content were observed to be almost the same square nanoplates, which indicates that the doping of Ln<sup>3+</sup> did not induce significant change in the size and morphology of NCs.

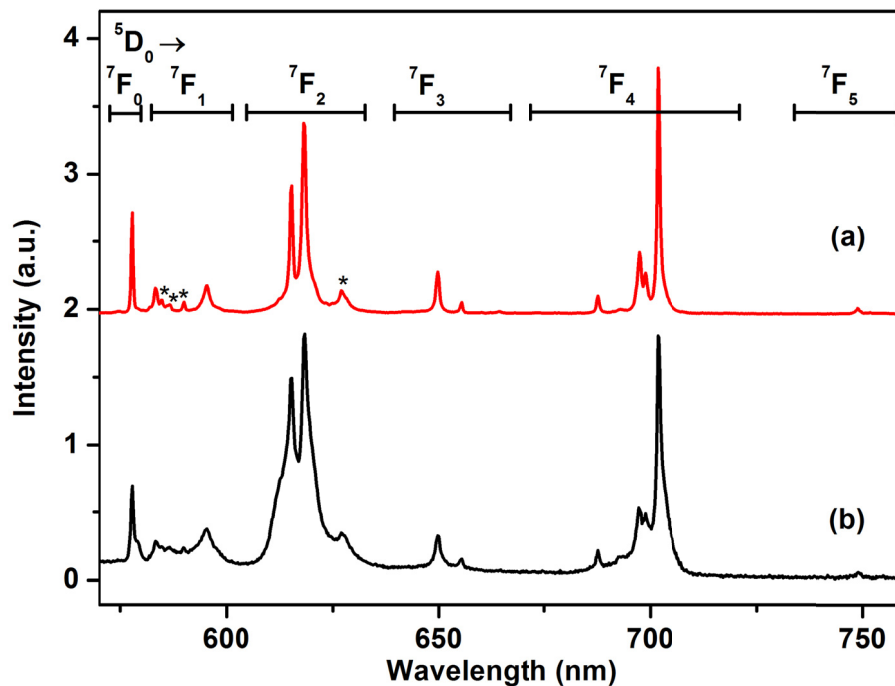


**Fig. S3** Room-temperature (RT) emission spectra of LaOBr:Eu<sup>3+</sup> (2 mol%) NCs upon excitation at (a) 303.0 nm corresponding to the charge-transfer (CT) band, and (b) 393.8 nm corresponding to the  ${}^7F_0 \rightarrow {}^5L_6$  transition of Eu<sup>3+</sup>, respectively. Upon excitation at 303.0 nm, characteristic sharp emission peaks centered at 577.9, 595.5, 618.2, 649.8, 701.7 and 748.8 nm attributed to the  ${}^5D_0$  to  ${}^7F_J$  ( $J=0, 1, 2, 3, 4, 5$ ) transitions of Eu<sup>3+</sup> can be observed. Peaks assigned to the  ${}^5D_1 \rightarrow {}^7F_J$  transitions were marked as star symbols. Interestingly, upon 393.8-nm excitation, much broader emission bands were observed.

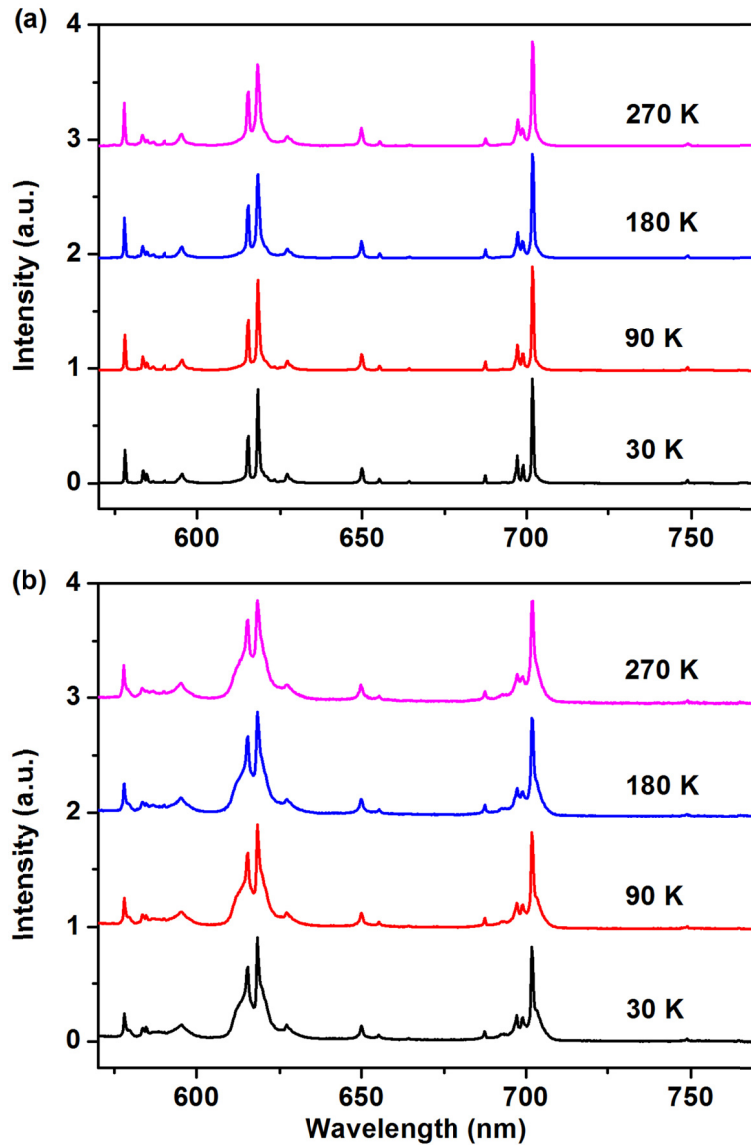


**Fig. S4** PL emission spectra of LaOBr:Eu<sup>3+</sup> (2 mol%) NCs upon excitation at (a) 303.0 and (b) 393.8 nm from 30 to 270 K. Upon excitation at 393.8 nm, the emission bands are still broad even at 30 K, which rules out the effect of thermal broadening at RT. As such, it is deduced that Eu<sup>3+</sup> ions in the as-prepared LaOBr NCs might occupy more than one type of sites.

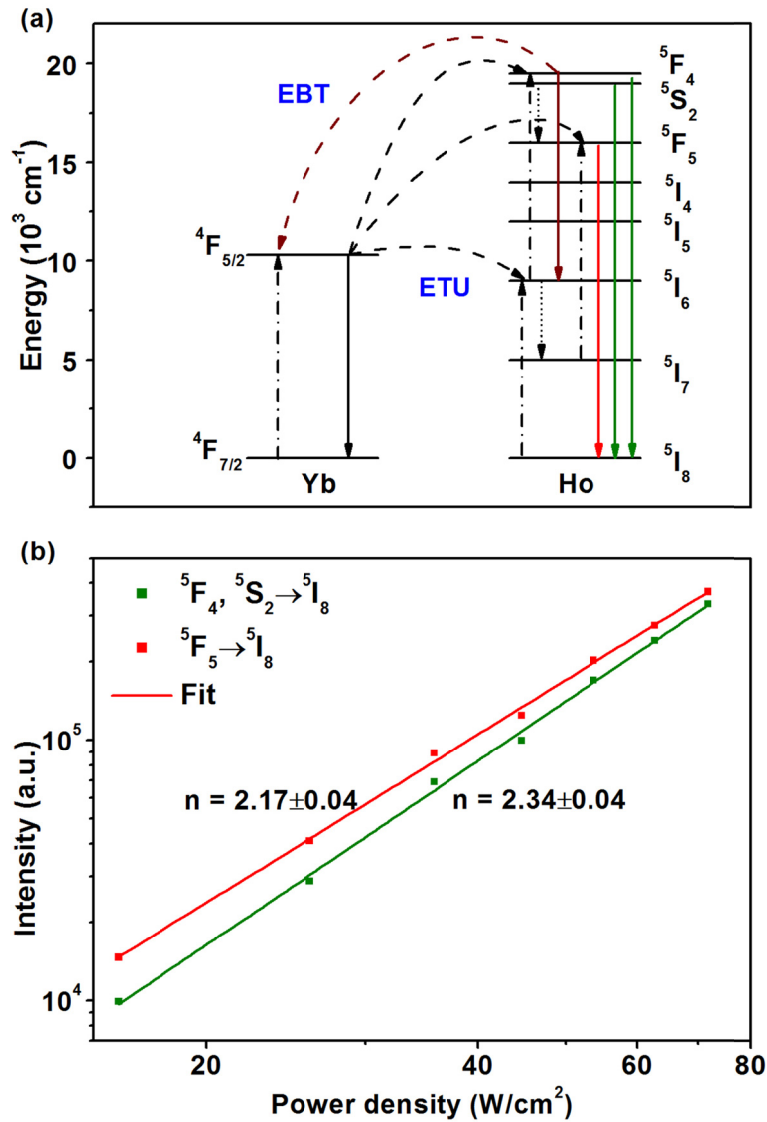


**Fig. S5** (a) Energy-level diagram showing upconversion (UC) processes for  $\text{Ho}^{3+}$  through sensitization of  $\text{Yb}^{3+}$ . The dash-dotted, dashed, dotted, and full arrows represent photon excitation, energy transfer, multiphonon relaxation, and emission processes, respectively. For  $\text{LaOBr}:\text{Yb}^{3+}/\text{Ho}^{3+}$ , the UC luminescence is mainly based on the energy transfer UC (ETU) process, where  $\text{Yb}^{3+}$  sequential absorbs two photons and transfers the energy to the neighboring  $\text{Ho}^{3+}$  followed by UC emission. As the doped concentration of  $\text{Yb}^{3+}$  increases, more efficient energy back transfer (EBT) from  $\text{Ho}^{3+}$  to  $\text{Yb}^{3+}$  happens:  $5S_2(\text{Ho}^{3+}) + 2F_{7/2}(\text{Yb}^{3+}) \rightarrow 5I_6(\text{Ho}^{3+}) + 2F_{5/2}(\text{Yb}^{3+})$ . (b) Log-log plots of the UC emission intensity versus near-infrared (NIR) excitation power density for  $\text{LaOBr}:\text{Yb}^{3+}/\text{Ho}^{3+}$  (20/2 mol%) NCs. The slopes for  $5F_5$  and the thermally coupled  $5F_4/5S_2$  multiplets to  $5I_8$  transitions of  $\text{Ho}^{3+}$  were determined to be  $2.17 \pm 0.04$  and  $2.34 \pm 0.04$ , respectively, which demonstrates that both UC emissions occurred via a two-photon process.

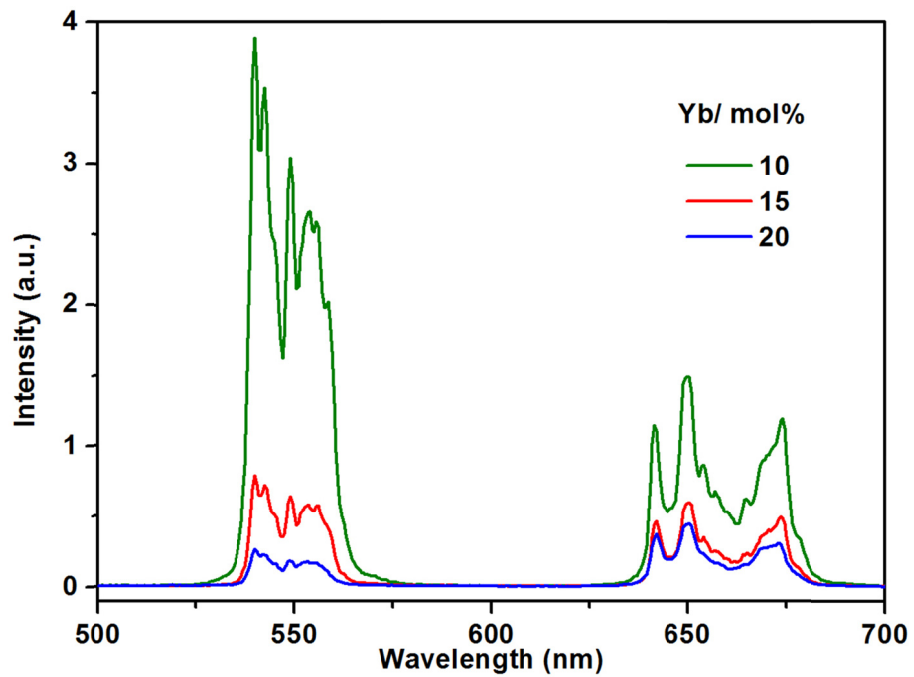


**Fig. S6** UC spectra of LaOBr:Yb<sup>3+</sup>/Ho<sup>3+</sup> (10, 15, 20/2 mol%) NCs. Both the red and green emissions became weaker as the doped concentration of Yb<sup>3+</sup> increased from 10 to 15, 20 mol% in LaOBr:Yb<sup>3+</sup>/Ho<sup>3+</sup> NCs.

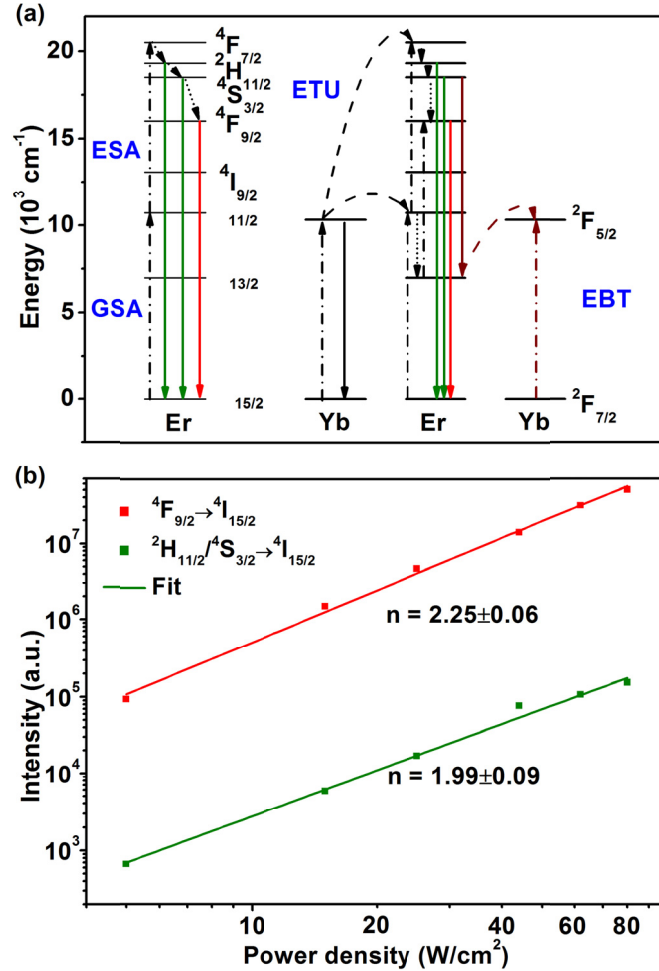


**Fig. S7** (a) Energy-level diagrams showing UC processes for Er<sup>3+</sup> and Yb<sup>3+</sup>/Er<sup>3+</sup> doped LaOBr NCs, respectively. The dash-dotted, dashed, dotted, and full arrows represent photon excitation, energy transfer, multiphonon relaxation, and emission processes, respectively. For LaOBr:Er<sup>3+</sup>, the UC luminescence is based on the ground state absorption (GSA) and excited state absorption (ESA) processes, where Er<sup>3+</sup> absorbs one photon to excite the ground state (<sup>4</sup>I<sub>15/2</sub>) to the first excited state (<sup>4</sup>I<sub>11/2</sub>), then absorbs another photon to reach the second excited state (<sup>4</sup>F<sub>7/2</sub>) followed by UC emission. For LaOBr:Yb<sup>3+</sup>/Er<sup>3+</sup>, the UC luminescence is mainly based on the ETU process, where Yb<sup>3+</sup> sequential absorbs two photons and transfers the energy to the neighboring Er<sup>3+</sup> followed by UC emission. As the doped concentration of Yb<sup>3+</sup> increases, more efficient EBT from Er<sup>3+</sup> to Yb<sup>3+</sup> happens: <sup>4</sup>S<sub>3/2</sub>(Er<sup>3+</sup>) + <sup>2</sup>F<sub>7/2</sub>(Yb<sup>3+</sup>) → <sup>4</sup>I<sub>13/2</sub>(Er<sup>3+</sup>) + <sup>2</sup>F<sub>5/2</sub>(Yb<sup>3+</sup>). (b) Log-log plots of the UC emission intensity versus NIR excitation power density for LaOBr:Yb<sup>3+</sup>/Er<sup>3+</sup> (5/2 mol%) NCs. The slopes for the UC emissions from <sup>4</sup>F<sub>9/2</sub> and the thermally coupled <sup>2</sup>H<sub>11/2</sub>/<sup>4</sup>S<sub>3/2</sub> multiplets to <sup>4</sup>I<sub>15/2</sub> were determined to be 2.25 ± 0.06 and 1.99 ± 0.09, respectively, which demonstrates that both emissions were realized via a two-photon process.

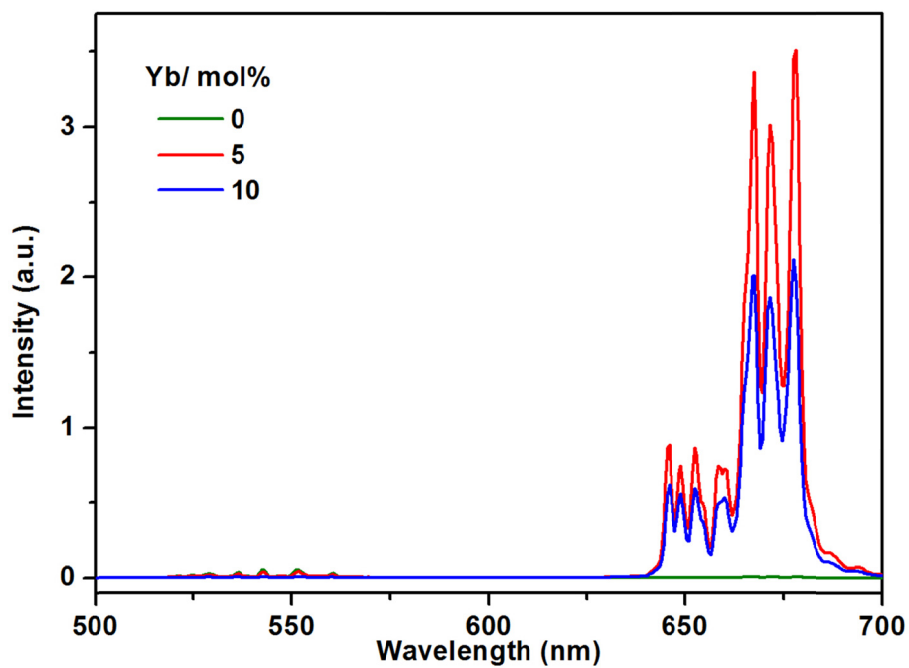


**Fig. S8** UC spectra of LaOBr:Yb<sup>3+</sup>/Er<sup>3+</sup> (0, 5, 10/2 mol%) NCs. The overall luminescence intensity decreased with the doped concentration of Yb<sup>3+</sup> increasing from 5 to 10 mol%.

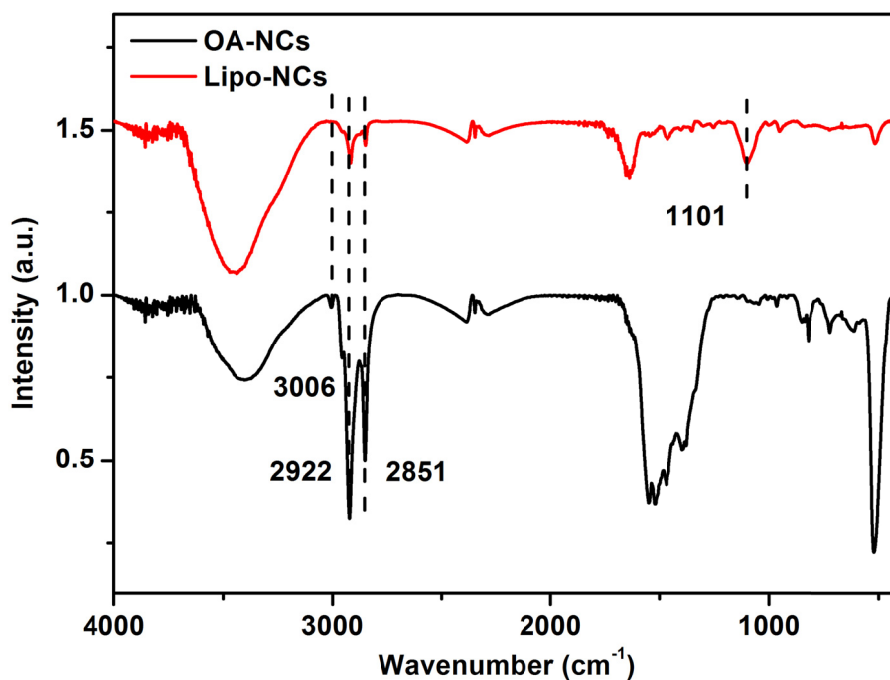


**Fig. S9** Fourier transform infrared (FTIR) spectra for oleic acid (OA) and 1,2-distearoyl-sn-glycero-3-phosphoethanolamine-N-[methoxy(polyethyleneglycol)-2000] (DSPE-PEG) phospholipid (Lipo) capped LaOBr NCs. In the FTIR spectrum of OA-NCs, the peak at 3006 cm<sup>-1</sup> was attributed to the C-H stretching vibration, and peaks at 2922 and 2851 cm<sup>-1</sup> were attributed to the asymmetric and symmetric stretching vibrations of -CH<sub>2</sub>- in the long alkyl chain of OA. After surface coating with functional phospholipids, a new peak of 1101 cm<sup>-1</sup> ascribed to asymmetric stretching of C-O-C from PEG appeared, indicating that the DSPE-PEG phospholipid was successfully assembled on the OA-NCs surface via self-assembly.

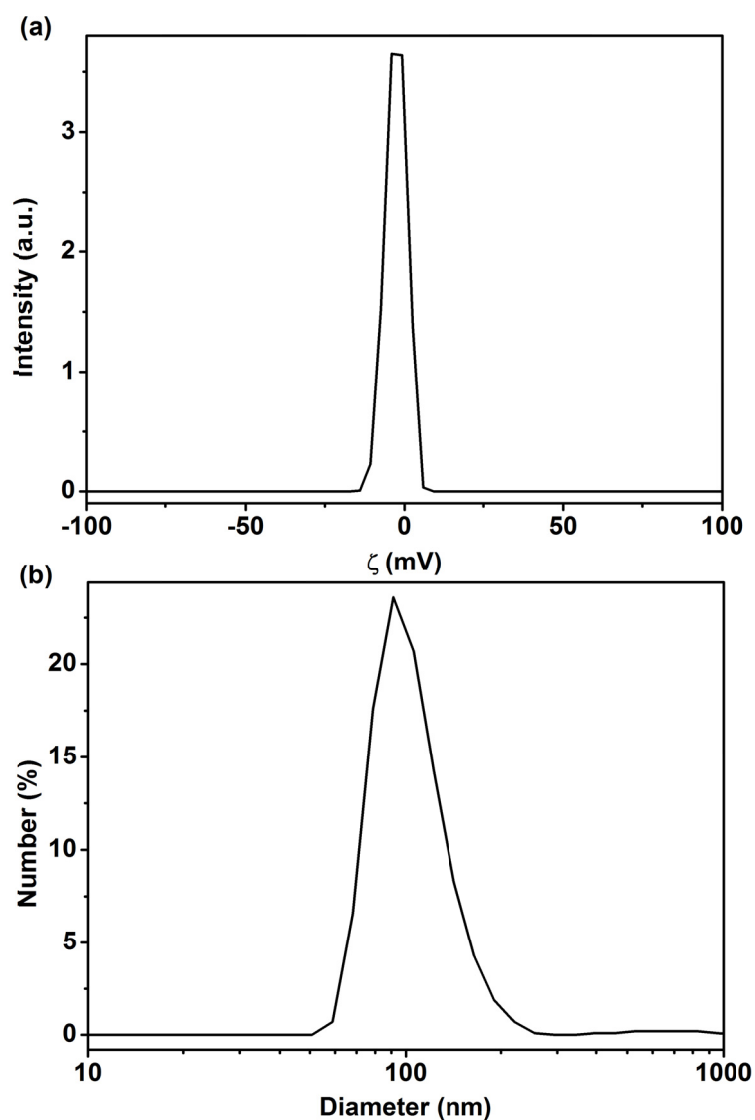


**Fig. S10** (a)  $\zeta$ -potential of Lipo-LaOBr NCs dispersed in water. The  $\zeta$ -potential was determined to be -4.5 mV, confirming the successful conjugation of DSPE-PEG phospholipid on the surface of the NCs. (b) Hydrodynamic diameter distribution of Lipo-LaOBr NCs dispersed in water (pH = 7.0). The mean hydrodynamic diameter was determined to be 91.4 nm. In comparison with the OA-capped NCs (74 nm), the increase of ~17 nm in diameter is due to the existence of monolayer PEGylated phospholipids.

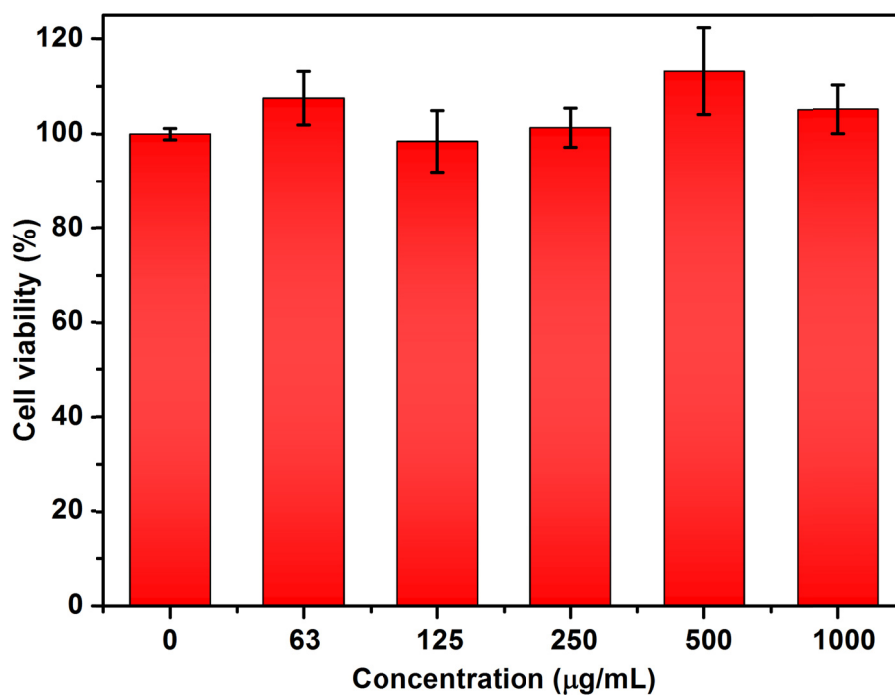


**Fig. S11** Viability of human embryo lung fibroblasts (HELF) cells after incubating with Lipo-LaOBr:Yb<sup>3+</sup>/Er<sup>3+</sup> NCs. The HELF cells were grown with the medium containing different concentrations of NCs for 24 h, and the cell viability was determined on the basis of methylthiazolyltetrazolium (MTT) assay. The viability of untreated cells without the addition of NCs was assumed to be 100%. Upon incubation with NCs, the cell viability still remained above 95% even at high concentrations (1000 µg/mL) of NCs, which indicates that the Lipo-NCs are biocompatible and essentially nontoxic to live cells, allowing for safe luminescent biosensing.